FEATURE ARTICLE

Quantum Dissipative Dynamics: A Numerically Exact Methodology

Nancy Makri

School of Chemical Sciences, University of Illinois, 601 S. Goodwin Avenue, Urbana, Illinois 61801

Received: December 1, 1997; In Final Form: February 26, 1998

A fully quantum mechanical methodology for simulating the time evolution of low-dimensional systems in harmonic dissipative environments is presented. The key features of the method are the numerical construction of accurate propagators based on physically motivated reference Hamiltonians and the decomposition of the path integral into a series of shorter time operations, which leads to an iterative algorithm. Illustrative applications to barrier-crossing events and biological electron transfer are presented.

I. Introduction

The introduction in the last two decades of advanced spectroscopic techniques with subpicosecond temporal resolution has had an unprecedented impact on the way chemists view molecular processes. The emerging picture has been made more clear with the aid of computer modeling. In particular, the use of classical molecular dynamics simulations has offered detailed pictures of molecular collisions and rearrangements, while the advent of quantum time-evolution algorithms has contributed significantly to the understanding of classically forbidden effects. Unfortunately, rigorous quantum mechanical simulations are presently limited to small molecules.

This article deals with the quantum dynamics of condensed-phase phenomena. We focus on processes that occur in phonon environments and are modulated by the interaction of the system of interest with the collective vibrations of its surrounding host. As an example, consider the dynamics (e.g., vibrational relaxation or tunneling between two equivalent configurations) of a molecular impurity in a crystalline solid. If the internal degrees of freedom of the isolated impurity pertaining to the process of interest can be described by a Hamiltonian H_s, the total Hamiltonian can be written in the form

$$H = H_s + \sum_j \left(\frac{P_j^2}{2m_j} + \frac{1}{2} m\omega_j^2 x_j^2 - f_j(s) x_j \right) \qquad (1.1)$$

Here s denotes the coordinate(s) of the system of interest and x_j are harmonic "bath" degrees of freedom representing the phonons of the environment. Interaction between system and bath is described through the coupling functions $f_j(s)$; the coupling term is chosen linear in the phonon coordinates, representing the lowest nontrivial term in the Taylor series expansion of the potential. In many situations the coupling is linearized with respect to the system coordinate as well, i.e., one takes $f_j(s) = c_j s$, although this is not an essential requirement to the methodology described below. It is assumed that the properties of the system can be probed experimentally (e.g., via spectroscopic techniques), while the large number of phonon vibrations are of interest only to the extent that they affect the dynamics of the system.

Having stated the above preliminaries, the goal is to calculate the time evolution of observables pertaining to the system in the presence of coupling to the medium at a given temperature. It is known that interaction with a macroscopic bath has profound consequences on the properties of the observable system. In general, these include irreversibility and at least some degree of decoherence, such that the ensuing dynamics often bears little resemblance to that of the isolated molecule. The fact that molecular eigenstates are not eigenstates of the total Hamiltonian leads to dephasing and population relaxation, characterized by the flow of energy out of excited states of the system until Boltzmann equilibrium is established. Tunneling splittings are usually shifted to lower frequencies, and coherent tunneling oscillations are under certain conditions replaced by rate dynamics.

Clearly, direct solution of the Schrödinger equation with the multidimensional Hamiltonian of eq 1.1 is computationally prohibitive. An equally rigorous alternative is the use of Feynman's path integral formulation of time-dependent quantum mechanics.[1,2] In Feynman's approach a transition amplitude or propagator is expressed as a sum of amplitudes along all paths that connect the initial and final points. Each of these amplitudes is a complex number with phase equal to the classical action along a path measured in units of Planck's constant. In the classical limit the phase is generally very large and the amplitude a highly oscillatory functional of the path such that the contributions from most paths sum to zero. Classical trajectories, the phase of which is stationary, constitute an exception; paths within a tube of width on the order of $\hbar$ around each classical trajectory add up constructively in this limit, and one recovers the semiclassical result where the propagator is expressed in terms of purely classical components.[2]

From a numerical standpoint, performing the sum over Feynman paths represents a formidable task due to phase cancellation. The conventional parametrization of paths is in terms of straight line segments: one divides the total propagation time into N time slices of length $\Delta t = t/N$ and expresses the propagator in terms of an $N-1$-dimensional integral involving

S1089-5639(98)00359-4 CCC: $15.00
Published on Web 05/22/1998

shorter time propagators. The drawback of this approach is that it requires a very fine discretization. At the same time, all short time propagators enter with the same weight but rapidly varying phases; as a consequence, Monte Carlo sampling generally fails to yield converged results. A number of schemes have been proposed in the last decade for dealing with the massive phase cancellation problem that hinders evaluation of the real-time path integral. These include analytic continuation[3] or inversion[4,5] of imaginary-time quantities, stochastic sampling of the complex time propagator about classical paths,[6−12] stationary phase filtering,[13−20] construction of smooth propagators,[21−23] and recursive schemes based on cumulant expansions of path class averages.[24] These methods have been partially successful, but their applications are limited. To date, no stable simulation methods are known that are capable of obtaining quantum dynamical properties of arbitrary many-particle systems over long times. However, recent progress has led to a stable fully quantum mechanical algorithm for calculating the dynamics of systems in contact with dissipative baths of the type described by eq 1.1. This methodology is reviewed below and illustrated with examples describing its use to explore the dynamics of classically forbidden phenomena, such as tunneling and electronically nonadiabatic events.

Section II describes the path integral representation of the reduced density matrix, introducing an improved propagator based on a physically motivated zeroth Hamiltonian which is chosen to reflect the specifics of the motion on the one-dimensional adiabatic path. The same section discusses optimal quadratures for the evaluation of the resulting path integral expressions. Section III presents a decomposition of the path integral which leads to an iterative algorithm. Tunneling of impurities in solid hosts is discussed in section IV in the context of reaction rate theory and the dissipative two-state model. That section also describes the application of this methodology to electron-transfer processes and illustrates it with the example of primary charge separation in bacterial photosynthetic reaction centers. Finally, a summary and a brief outlook appear in section V.

II. The Path Integral: Adiabatic Reference and Discrete Variable Representation

The evolution of observables pertaining to the system of interest is most effectively expressed in terms of the reduced density matrix,

$$\tilde{\rho}(s'',s';t) \equiv \mathrm{Tr}_{\mathrm{bath}}\langle s''|\mathrm{e}^{-\mathrm{i}Ht/\hbar}\rho(0)\mathrm{e}^{\mathrm{i}Ht/\hbar}|s'\rangle \qquad (2.1)$$

Here the trace is evaluated with respect to all the bath degrees of freedom $\{x_i\}$ and $\rho(0)$ is the initial density operator. It is often assumed that the system and bath are uncorrelated at $t = 0$, such that the density operator factorizes:

$$\rho(0) = \rho_s(0)\,\rho_{\mathrm{bath}}(0) \qquad (2.2)$$

Below we adopt this form for convenience, although the last assumption is not essential to the methodology that follows.

The discretized path integral representation is obtained by splitting the time into N increments of length $\Delta t = t/N$ and replacing the exponential of the sum by the product of exponentials:

$$\tilde{\rho}(s'',s';N\Delta t) = \mathrm{Tr}_{\mathrm{bath}}\langle s''|\mathrm{e}^{-\mathrm{i}H\Delta t/\hbar}\mathrm{e}^{-\mathrm{i}H\Delta t/\hbar}...\mathrm{e}^{-\mathrm{i}H\Delta t/\hbar}\rho(0)\mathrm{e}^{\mathrm{i}H\Delta t/\hbar}\mathrm{e}^{\mathrm{i}H\Delta t/\hbar}...\mathrm{e}^{\mathrm{i}H\Delta t/\hbar}|s'\rangle \qquad (2.3)$$

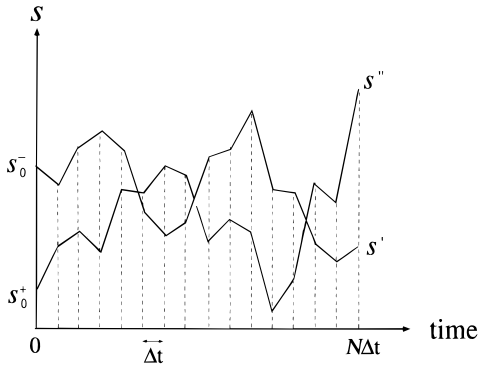

Figure 1. Discretized system path in forward−backward time entering the path integral representation of the reduced density matrix, eq 2.4.

Repeated insertion of the resolution of identity in terms of complete sets of system coordinate states leads to the following path integral expression:

$$\tilde{\rho}(s'',s';N\Delta t) = \mathrm{Tr}_{\mathrm{bath}}\int \mathrm{d}s_0^+ \int \mathrm{d}s_1^+ ... \int \mathrm{d}s_{N-1}^+ \int \mathrm{d}s_0^- \int \mathrm{d}s_1^- ... \int \mathrm{d}s_{N-1}^- \langle s''|\mathrm{e}^{-\mathrm{i}H\Delta t/\hbar}|s_{N-1}^+\rangle\langle s_{N-1}^+|\mathrm{e}^{-\mathrm{i}H\Delta t/\hbar}|s_{N-2}^+\rangle ... \langle s_1^+|\mathrm{e}^{-\mathrm{i}H\Delta t/\hbar}|s_0^+\rangle\langle s_0^+|\rho_s(0)|s_0^-\rangle\langle s_0^-|\mathrm{e}^{\mathrm{i}H\Delta t/\hbar}|s_1^-\rangle \times \langle s_1^-|\mathrm{e}^{\mathrm{i}H\Delta t/\hbar}|s_2^-\rangle ... \langle s_{N-1}^-|\mathrm{e}^{\mathrm{i}H\Delta t/\hbar}|s'\rangle \qquad (2.4)$$

The last equation is exact for any value of N. The sequences $s_0^+, s_1^+, ..., s_N^+$ and $s_0^-, s_1^-, ..., s_N^-$ (where $s_N^+ \equiv s''$ and $s_N^- \equiv s'$) define discrete system paths in forward and backward time (see Figure 1). Notice that each of the short time propagators in eq 2.4 is still an operator in the space of the bath degrees of freedom.

To allow numerical evaluation, the propagators in eq 2.4 must be available in some form. This requirement dictates an approximate factorization of the short time evolution operator into components whose propagators can be obtained either analytically or numerically. Traditionally, this factorization utilizes the kinetic energy K_s of the quantum system (or of all degrees of freedom) as the reference:

$$\langle s_{k''}|\mathrm{e}^{-\mathrm{i}H\Delta t/\hbar}|s_{k'}\rangle \approx \langle s_{k''}|\mathrm{e}^{-\mathrm{i}(H-K_s)\Delta t/2\hbar}\mathrm{e}^{-\mathrm{i}K_s\Delta t/\hbar}\mathrm{e}^{-\mathrm{i}(H-K_s)\Delta t/2\hbar}|s_{k'}\rangle \qquad (2.5)$$

$$= \sqrt{\frac{m}{2\pi\mathrm{i}\hbar\Delta t}}\mathrm{e}^{\mathrm{i}m(s_{k''}-s_{k'})^2/2\hbar\Delta t} \times \mathrm{e}^{-\mathrm{i}[H(s_{k''})-K_s]\Delta t/2\hbar}\mathrm{e}^{-\mathrm{i}[H(s_{k'})-K_s]\Delta t/2\hbar}$$

Because the kinetic energy operator does not commute with the potential terms in the Hamiltonian, the last equation is valid only in the limit of vanishing time step. As a consequence, one must use a large number of time slices for a given total time t, leading to a high-dimensional path integral expression. Numerical evaluation of such integrals is problematic due to the rapidly oscillatory nature of the short time propagators in eq 2.5. Because eq 2.5 arises from artificial separation of the system Hamiltonian into noncommuting kinetic and potential energy parts, the problems associated with the multidimensional character of the primitive path integral representation persist even in the absence of system−bath coupling.

A superior path integral representation of the reduced density matrix emerges if one employs a physically motivated reference. Depending on the system, several choices are possible which include judiciously constructed or even variationally optimized

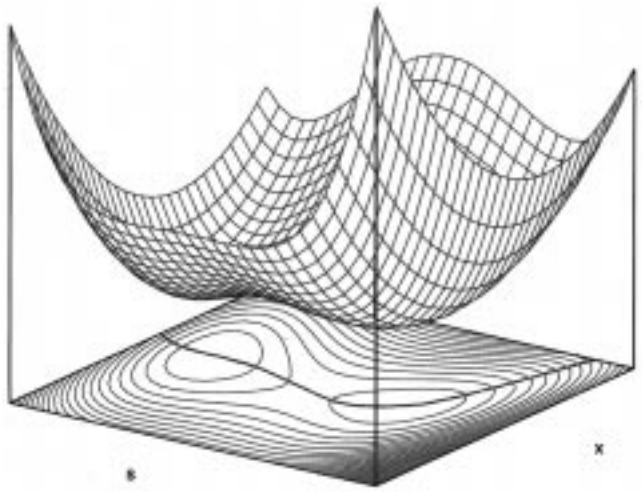

Figure 2. Typical potential energy surface described by eq 1.1 in the case where the bath consists of a single-harmonic oscillator. The adiabatic path is indicated via the purple line.

reference potentials. A simple, yet computationally advantageous reference is given by the Hamiltonian along the one-dimensional adiabatic path:[25]

$$H_0 = H_s - \sum_j \frac{f_j(s)^2}{2m_j\omega_j^2} \tag{2.6}$$

Unlike the primitive reference used in eq 2.5, the last equation includes the kinetic energy of the quantum particle *as well as the full potential* the latter experiences on the adiabatic path $x_j = f_j(s)/m_j\omega_j^2$. This line is defined by the points of lowest potential energy at each fixed position of the system, as illustrated in Figure 2. In the limit where the bath responds infinitely faster than the system, the walls surrounding the potential valley become infinitely steep and the dynamics is governed by the motion on the adiabatic path.

The adiabatic reference introduced in eq 2.6 is both physically appealing and sufficiently simple such that it can be dealt with exactly. At the same time, the remaining Hamiltonian

$$H - H_0 = \sum_j \frac{P_j^2}{2m_j} + \frac{1}{2}m_j\omega_j^2\left(x_j - \frac{f_j(s)}{m_j\omega_j^2}\right)^2 \tag{2.7}$$

consists of linearly displaced harmonic oscillators whose quantum mechanics is readily available. By using a symmetric splitting of the short time evolution operator and taking advantage of the parametric dependence of the displaced bath Hamiltonian on the system coordinate, one arrives at the following product form of the system−bath propagator:

$$\langle s_{k''}|e^{-iH\Delta t/\hbar}|s_{k'}\rangle \approx \langle s_{k''}|e^{-iH_0\Delta t/\hbar}|s_{k'}\rangle e^{-i[H-H_0(s_{k''})]\Delta t/2\hbar} e^{-i[H-H_0(s_{k'})\Delta t]/2\hbar} \tag{2.8}$$

The only source of error in the last equation is the nonvanishing commutator between the kinetic energy of the system and the system−bath coupling functions present in $H - H_0$. This error can be brought in the form of the following nested commutator:

$$\left[\frac{p_s^2}{2m_0},\left[\frac{p_s^2}{2m_0},\sum_j\left(x_j - \frac{f_j(s)}{m_j\omega_j^2}\right)^2\right]\right]\Delta t^3 \tag{2.9}$$

As seen from this expression, eq 2.8 is exact for *any* time step not only for the uncoupled Hamiltonian but also with finite system−bath coupling in the case of an infinite frequency phonon spectrum. In the latter case the motion is confined to the narrow valley surrounding the adiabatic path and nonadiabatic corrections are negligible. In the realistic case of a bath with high, though finite frequencies and/or weak to moderate coupling strength, eq 2.8 provides an excellent approximation even with sizable time steps.

Interestingly, the quasi-adiabatic partitioning of the propagator according to eq 2.8 is accurate also in the opposite limit of a sluggish bath. This is so because the period of the bath oscillators is very large in this case, such that large but finite time steps provide adequate discretization. In fact, the details of partitioning the system−bath Hamiltonian are irrelevant in the limit of a zero-frequency bath as long as the kinetic and potential energy terms of each degree of freedom are not separated.

Having identified a physically appealing reference which leads to a superior partitioning of the propagator, one can formally express the reduced density matrix as

$$\begin{aligned}\tilde{\rho}(s'',s';N\Delta t) = \int ds_0^+ \int ds_1^+ ... \int ds_{N-1}^+ \int ds_0^- \int ds_1^- ... \\ \int ds_{N-1}^- \langle s''|e^{-iH_0\Delta t/\hbar}|s_{N-1}^+\rangle\langle s_{N-1}^+|e^{-iH_0\Delta t/\hbar}|s_{N-2}^+\rangle ... \\ \langle s_1^+|e^{-iH_0\Delta t/\hbar}|s_0^+\rangle\langle s_0^+|\rho_s(0)|s_0^-\rangle \times \\ \langle s_0^-|e^{iH_0\Delta t/\hbar}|s_1^-\rangle\langle s_1^-|e^{iH_0\Delta t/\hbar}|s_2^-\rangle ... \langle s_{N-1}^-|e^{iH_0\Delta t/\hbar}|s'\rangle \times \\ F(s_0^+,s_1^+,...,s_N^+,s_0^-,s_1^-,...,s_N^-)\end{aligned} \tag{2.10}$$

Here

$$\begin{aligned}F(s_0^+,s_1^+,...,s_N^+,s_0^-,s_1^-,...,s_N^-) = \\ \mathrm{Tr}_{\mathrm{bath}}\left\{\exp\left(-\frac{i}{\hbar}\frac{\Delta t}{2}[H - H_0(s'')]\right)\exp\left(-\frac{i}{\hbar}\Delta t[H - H_0(s_{N-1}^+)]\right)...\exp\left(-\frac{i}{\hbar}\frac{\Delta t}{2}[H - H_0(s_0^+)]\right) \times \right. \\ \rho_{\mathrm{bath}}(0)\exp\left(\frac{i}{\hbar}\frac{\Delta t}{2}[H - H_0(s_0^-)]\right) \times \\ \left.\exp\left(\frac{i}{\hbar}\Delta t[H - H_0(s_1^-)]\right)...\exp\left(\frac{i}{\hbar}\frac{\Delta t}{2}[H - H_0(s')]\right)\right\}\end{aligned} \tag{2.11}$$

is an "influence functional" of system forward and backward paths. Since the relevant Hamiltonian consists of linearly displaced harmonic oscillators, F can be evaluated analytically. For a Boltzmann ensemble described by the density operator

$$\rho_{\mathrm{bath}}(0) = \frac{\exp(-\beta H_{\mathrm{bath}})}{\mathrm{Tr}\exp(-\beta H_{\mathrm{bath}})} \tag{2.12}$$

where H_{bath} is the Hamiltonian of the bare medium, and for bilinear system−bath coupling of the type

$$f_j(s) = c_j s \tag{2.13}$$

use of the procedure described by Feynman and Vernon[26] leads to the result

$$F = \exp\left(-\frac{1}{\hbar}\sum_{k=0}^{N}\sum_{k'=0}^{k}(s_k^+ - s_k^-)(\eta_{kk'}s_{k'}^+ - \eta_{kk'}^*s_{k'}^-)\right) \tag{2.14}$$

Here $\eta_{kk'}$ are complex-valued coefficients that depend on the collective characteristics of the medium via integrals involving the bath spectral density

$$J(\omega) = \frac{\pi}{2}\sum_j \frac{c_j^2}{m_j\omega_j}\delta(\omega - \omega_j) \quad (2.15)$$

and have been given explicitly in ref 27. For example, for $0 < k,k' < N$, one finds

$$\eta_{kk'} = \frac{2}{\pi}\int_{-\infty}^{\infty} d\omega \frac{J(\omega)}{\omega^2} \frac{\exp(^1/_2\hbar\omega\beta)}{\sinh(^1/_2\hbar\omega\beta)} \times \sin^2(\omega\Delta t/2)\exp(-i(k-k')\omega\Delta t) \quad (2.16)$$

where the spectral density at negative frequencies is defined as an odd function. These results can be extended to Hamiltonians with arbitrary coupling functions $f_j(s)$ and to initial conditions including system−bath correlation, although the resulting expressions are slightly more complicated.

The spectral density function is the coupling-weighted density of states of the phonon bath. If the environment consists of only a few degrees of freedom, as in the case of a small organic molecule, $J(\omega)$ is composed of delta function-like peaks. Broad spectral densities are characteristic of macroscopic media (solids, liquids, or large biological molecules) and are responsible for loss. In order for system relaxation to occur via first-order processes, this function must overlap with the characteristic frequencies of the quantum system; otherwise transitions can take place only via multiphonon effects and the ensuing decay is slow.

The final component required in eq 2.8 is the short time propagator for the reference Hamiltonian. For a general nonlinear potential this propagator must be evaluated numerically. Use of the spectral expansion of the time evolution operator leads to the identity

$$\langle s_{k''}|e^{-iH_0\Delta t/\hbar}|s_{k'}\rangle = \sum_{n=0}^{n_{max}} \Phi_n(s_{k''})\,\Phi_n(s_{k'})\,e^{-iE_n\Delta t/\hbar} \quad (2.17)$$

where Φ_n and E_n are, respectively, the eigenfunctions and eigenvalues of the reference Hamiltonian H_0 and $n_{max} \rightarrow \infty$. The practical question that arises immediately is whether eq 2.17 can be evaluated using a finite number of eigenstates. Since the terms in eq 2.17 oscillate in phase but do not decay in magnitude with increasing quantum number, such truncation is strictly incorrect if one is concerned with recovering the reference propagator exactly. Notice, however, that the specifics of the propagator need to be reproduced only to the extent that they affect the reduced density matrix via eq 2.8. As the latter involves integrals of short time propagators over one or both endpoints, contributions from high-energy states become progressively smaller as Φ_n overlap less with the initial density matrix. This observation allows truncation[25] of the sum in eq 2.17 at some finite n_{max}, and convergence is usually exponential with this parameter. The additional advantage gained by this representation of the reference propagator is the large-scale smoothing achieved by the omission of rapidly oscillatory high-energy components. Furthermore, the truncated reference propagator is spatially confined to the regions characterized by significant wave function amplitude.[22] Both of these features are extremely desirable for the numerical evaluation of the reduced density matrix. The effective propagator for a Morse oscillator is illustrated in Figure 3 for two values of n_{max}.

Equation 2.10, with the influence functional given by eq 2.14 and the reference propagator constructed numerically according to eq 2.17, is the *quasi-adiabatic propagator path integral*

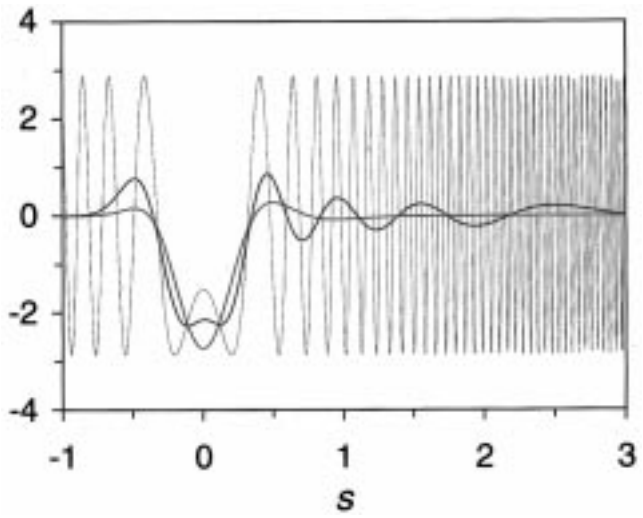

Figure 3. Short time propagators plotted vs one of the endpoints for a system described by a Morse potential. The other endpoint is fixed at $s = 0$, which corresponds to the potential minimum. The time step is equal to a tenth of the vibrational period at the potential minimum. Red line: effective propagator constructed in terms of the lowest six energy eigenstates. Blue line: effective propagator constructed in terms of the lowest 12 energy eigenstates. The fine black line shows the primitive propagator obtained by partitioning the Hamiltonian into kinetic and potential energy terms.

representation of the reduced density matrix for a quantum particle in a finite-temperature phonon bath.[25,28] This expression treats the dynamics along the adiabatic path exactly, nonadiabatic corrections entering via the influence functional. If such nonadiabatic corrections are small, eq 2.10 can converge with sizable time steps. In addition, the numerical construction of smooth and spatially localized reference propagators makes phase cancellation less severe.

Under certain favorable conditions (short time and strongly dissipative system−bath interactions) the presence of the influence functional, eq 2.14, damps sufficiently the slow oscillations of the effective reference propagators such that evaluation of the path integral by Monte Carlo methods is possible. In these cases the short time propagators in eq 2.8 are stored on a grid of points which defines the sampling domain for a multidimensional random walk.[25] In order to facilitate convergence in the presence of phase oscillations, the absolute value of the integrand is used as the sampling function, and the normalization integral of the latter is computed separately via umbrella sampling and related techniques.[29] This procedure converges well when the oscillations are relatively mild and the dimension of the integral is not very high.

In most other circumstances the oscillations in the integrand of the path integral expression are severe, and stochastic sampling methods fail to yield converged results with realistic amounts of numerical effort. The alternative use of multidimensional quadrature demands a judicious choice of grid points and can be successful only if the volume of integration is not very large, i.e., for small values of N. The more appealing iterative evaluation of the dynamics does not appear feasible due to the nonlocal interactions in the influence functional, i.e., the coupling of all integration variables in eq 2.8. As will be shown in the next section, the most promising scheme combines the use of optimal quadrature and a decomposition of the path integral which leads to an iterative algorithm. The remainder of this section describes a highly efficient grid representation.

To this end, we seek quadratures that require the smallest possible number of points per integration variable. Routine

discretization of coordinate space into uniform grids requires a minimum of 30−100 points per dimension and thus is prohibitive for all but the most trivial applications. Much more powerful tools arise from the use of Gaussian quadratures. However, the relevant transformation functions generally cannot be expressed in closed form when anharmonic potentials are involved.

Superior representations would be feasible if one could express the path integral in a noncoordinate basis. By construction, the reference propagators are diagonal in the basis of eigenstates Φ_n; as such, in the absence of system−bath coupling this basis would require no summations, except for those associated with the trace operation. Unfortunately, the eigenstate representation is not suitable for evaluation of the system−bath coupling part of the time-evolution operator, which is diagonal in the position basis.

An optimal representation arises from combining the attractive features of position space with those of the eigenstate basis, i.e, convergence with the same small number of terms as the eigenstate basis while diagonalizing the potential coupling. Such basis sets, known as discrete variable representations (DVRs), were introduced many years ago as convenient tools for evaluating potential matrix elements.[30,31] In the past decade, Light and co-workers extended the DVR idea to develop powerful methods for treating vibrational eigenvalue problems.[32−34] Uniform-grid discrete variable representations of the kinetic energy matrix and of the free particle propagator have been utilized recently in reactive scattering calculations.[35]

To apply the DVR idea in the path integral context, the system position operator is diagonalized in the basis of the M most relevant eigenstates of the reference Hamiltonian to construct the system-specific DVR states

$$u_n = \sum_{n'=1}^{M} L_{nn'}\Phi_{n'} \tag{2.18}$$

where the transformation coefficients are specified by the requirement

$$\langle u_n|s|u_{n'}\rangle = \sigma_n\delta_{nn'} \tag{2.19}$$

The states u_n constitute the discrete analogue of the ordinary coordinate states, and the eigenvalues σ_n, $n = 1, ..., M$ form the DVR grid. Representative illustrations of such states defined in terms of the eigenstates of a symmetric double-well potential are given in Figure 4. As the number of states employed in the DVR transformation increases, the DVR functions become more narrow and the corresponding grid denser, reflecting the closer resemblance of these functions to continuous position states. The DVR transformation is, in essence, a special system-tailored Gaussian quadrature. For example, Light has shown very clearly how the DVR corresponding to the angular part of an isotropic Hamiltonian is equivalent to the Gauss−Legendre quadrature.[32] Finally, note that the DVR basis is obtained via a unitary transformation of the eigenstate basis, and thus the DVR grid is sparse whenever the dynamics can be adequately represented by a small number of reference system eigenstates.

To make use of the DVR quadrature, one re-expresses the path integral using the resolution of identity in terms of the discretized position states,

$$1 = \int_{-\infty}^{\infty} ds_k|s_k\rangle\langle s_k| \approx \sum_{k_n=1}^{M} |u_{k_n}\rangle\langle u_{k_n}| \tag{2.20}$$

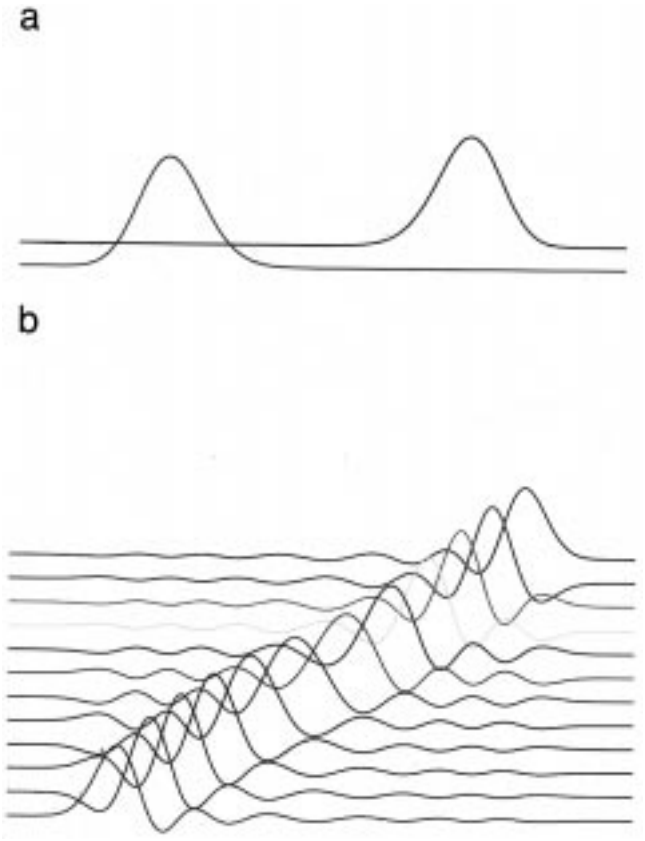

Figure 4. DVR states constructed from the M lowest lying states of a symmetric double-well potential: (a) $M = 2$; (b) $M = 12$.

This equation is numerically exact to the extent that the chosen states provide an adequate representation of the reduced density matrix for the coupled system−bath Hamiltonian (see also the discussion below) and allows the spectral expansion of the coupling present in the displaced bath time-evolution operator:

$$e^{-i(H-H_0)\Delta t/\hbar} = \sum_{k_n=1}^{M} |u_{k_n}\rangle e^{-i(H-H_0(\sigma_{k_n}))\Delta t/\hbar}\langle u_{k_n}| \tag{2.21}$$

The latter leads to the following DVR-discretized quasi-adiabatic propagator path integral representation of the reduced density matrix for the quantum particle:[36]

$$\begin{aligned}\tilde{\rho}(s'',s';N\Delta t) = \\ \sum_{k_0^+=1}^{M}\sum_{k_1^+=1}^{M}\cdots\sum_{k_{N-1}^+=1}^{M}\sum_{k_0^-=1}^{M}\sum_{k_1^-=1}^{M}\cdots\sum_{k_{N-1}^-=1}^{M} \langle s''|e^{-iH_0\Delta t/\hbar}|u_{k_{N-1}}^+\rangle \times \\ \langle u_{k_{N-1}}^+|e^{-iH_0\Delta t/\hbar}|u_{k_{N-2}}^+\rangle\cdots\langle u_{k_1}^+|e^{-iH_0\Delta t/\hbar}|u_{k_0}^+\rangle\langle u_{k_0}^+|\rho_s(0)|u_{k_0}^-\rangle \times \\ \langle u_{k_0}^-|e^{iH_0\Delta t/\hbar}|u_{k_1}^-\rangle\langle u_{k_1}^-|e^{iH_0\Delta t/\hbar}|u_{k_2}^-\rangle\cdots\langle u_{k_{N-1}}^-|e^{-iH_0\Delta t/\hbar}|s'\rangle \times \\ F(\sigma_{k_0}^+,\sigma_{k_1}^+,...,\sigma_{k_N}^+,\sigma_{k_0}^-,\sigma_{k_1}^-,...,\sigma_{k_N}^-)\end{aligned} \tag{2.22}$$

Because of the structure of eq 2.21, the influence functional remains unchanged in the DVR representation but is now evaluated at the new quadrature points. The DVR representation of the one-dimensional propagator for the adiabatic system Hamiltonian is constructed numerically with the aid of the basis transformation relations, eqs 2.18 and 2.19.

In the absence of system−bath coupling, the number M of terms required in eq 2.21 would be exactly equal to the minimum number n_{max} necessary for representing the dynamics of the quantum particle, i.e., the initial density matrix of the

system and the reference propagator. In the presence of system−bath interaction the DVR basis must be adequate for the expansion of the influence functional as well. Generally, eq 2.22 converges with values of M that are only slightly larger than n_{max}. The primitive, highly oscillatory propagator requires typically about 10^2-10^3 grid points per integration variable. Filtering out the high-energy components through the eigenstate expansion leads to smooth propagators that can be adequately represented with 30−100 coordinate points. Finally, in common situations typical of proton-transfer reactions the DVR quadrature makes the required number of integrand evaluations as small as 2−10 for each path integral variable. It is thus apparent that the introduction of system-specific DVR grids to the real-time path integral leads to a contraction of the multidimensional grid by a factor on the order of 100^{2N}. Finally, note that in situations involving unbound potentials or, more generally, whenever static basis functions cannot offer compact representations, efficient path integral quadratures can still be defined in terms of *time-dependent* discrete variable representations.[37] In such cases, the DVR basis functions will generally be different for different time points on a discrete path.

Apart from the significant practical advantages discussed above, the DVR representation of the path integral for the reduced density matrix provides a unified approach to the dynamics of quantum systems defined via continuous or discrete (lattice) Hamiltonians. A typical example is offered by symmetric proton-transfer reactions modeled in terms of one-dimensional double-well potentials. At very high temperatures the motion is nearly classical and the system must be modeled in terms of an extended coordinate. At the same time, high temperature allows population of highly excited system states, leading to a dense DVR grid. As the temperature is lowered, the number of relevant states decreases until one approaches a regime where the dynamics are dominated by the characteristics of the lowest tunneling doublet. Thus, the celebrated two-level system Hamiltonian emerges in the low-temperature limit simply from the use of only two system eigenstates in the DVR transformation of eq 2.18; no parameter rescaling is necessary, as the DVR states and eigenvalues carry all the necessary information.

To summarize the developments of this section, the DVR-discretized quasi-adiabatic propagator expression of the reduced density matrix for a quantum system interacting with a dissipative phonon environment offers the highly desirable features of convergence with relatively large time steps and sparse grid representation. These properties arise because the obtained path integral representation incorporates the exact dynamics along the adiabatic path as its zeroth-order limit and is spatially discretized via optimal system-specific quadratures. Still, with the exception of two- or three-level systems at relatively short times, evaluation of the resulting M^{2N}-dimensional integral is numerically prohibitive. This problem is dealt with in the next section.

III. Propagator Functional and Iterative Dynamics

In the absence of system−bath coupling the influence functional is equal to unity. In that limit the path integral representation of the reduced density matrix is equivalent to the time-dependent Schrödinger equation for the reference Hamiltonian. Indeed, the initial system density matrix can be expanded in the basis of its eigenstates as

$$\rho_s(0) = \sum_{n=1}^{n_{max}} a_n |\varphi_n\rangle\langle\varphi_n| \tag{3.1}$$

and the integrations in the resulting eq 2.8 for each term of the above expansion can be performed sequentially:

$$\langle s|\varphi_n((k+1)\Delta t)\rangle = \int_{-\infty}^{\infty} ds_k \langle s|e^{-iH_0\Delta t/\hbar}|s_k\rangle\langle s_k|\varphi_n(k\Delta t)\rangle, \quad k = 0, ..., N-1 \tag{3.2a}$$

Finally, after N propagation steps,

$$\langle s''|\rho_s(N\Delta t)|s'\rangle = \sum_{n=1}^{n_{max}} a_n \langle s''|\varphi_n(N\Delta t)\rangle\langle\varphi_n(N\Delta t)|s'\rangle \tag{3.2b}$$

As with any quantity satisfying a first-order differential equation with specified initial conditions, the dynamics of the density matrix is Markovian in the full Hilbert space of the Hamiltonian.

The situation described by eq 2.8 is significantly more complicated. Although the evolution of the full-dimensional system−bath density matrix $\rho(t) = \exp(-iHt/\hbar)\rho(0)\exp(iHt/\hbar)$ is still given by the first-order differential Schrödinger equation, the process of integrating out the bath to obtain the lower-dimensional reduced density matrix destroys the Markovian character of the dynamics. Within the path integral picture this occurs as the Feynman paths in the full path integral representation of the system−bath time-evolution operator,

$$\begin{aligned}\rho(s''\mathbf{x}'',s'\mathbf{x}';t) = &\int ds_0^+ \int ds_1^+ ... \\ &\int ds_{N-1}^+ \int ds_0^- \int ds_1^- ... \int ds_{N-1}^- \int d\mathbf{x}_0^+ \int d\mathbf{x}_1^+ ... \int d\mathbf{x}_{N-1}^+ \times \\ &\int d\mathbf{x}_0^- \int d\mathbf{x}_1^- ... \int d\mathbf{x}_{N-1}^- \langle s''\mathbf{x}''|e^{-iH\Delta t/\hbar}|s_{N-1}^+ \mathbf{x}_{N-1}^+\rangle \times \\ &\langle s_{N-1}^+ \mathbf{x}_{N-1}^+|e^{-iH\Delta t/\hbar}|s_{N-2}^+ \mathbf{x}_{N-2}^+\rangle ... \langle s_1^+ \mathbf{x}^+|e^{-iH\Delta t/\hbar}|s_0^+ \mathbf{x}_0^+\rangle \times \\ &\langle s_0^+ \mathbf{x}_0^+|\rho(0)|s_0^- \mathbf{x}_0^-\rangle \langle s_0^- \mathbf{x}_0^-|e^{iH\Delta t/\hbar}|s_1^- \mathbf{x}_1^-\rangle \times \\ &\langle s_1^- \mathbf{x}_1^-|e^{iH\Delta t/\hbar}|s_2^- \mathbf{x}_2^-\rangle ... \langle s_{N-1}^- \mathbf{x}_{N-1}^-|e^{iH\Delta t/\hbar}|s'\mathbf{x}'\rangle\end{aligned} \tag{3.3}$$

are projected on the system−time plane through the process of performing the integrals over the bath variables $\mathbf{x}_k$ (see Figure 5). The result is an influence functional of the system paths with nonlocal interactions, i.e., couplings between the variables $s_k^{\pm}$ and $s_{k'}^{\pm}$, which prevent decomposition of the reduced-dimension path integral into sequential integrations of the type shown in eq 3.2.

The nonlocal terms in the path integral expression of the reduced density matrix arise from the correlation function of the medium,[26]

$$\alpha(t-t') = \hbar^{-1}\sum_j c_j^2 \langle x_j(t')\, x_j(t)\rangle \tag{3.4}$$

which in the case of a harmonic bath takes the form

$$\begin{aligned}\alpha(t) &= \sum_j \frac{c_j^2}{2m_j\omega_j}[\coth(^1/_2\hbar\omega_j\beta)\cos(\omega_j t) - i\sin(\omega_j t)] \\ &= \frac{1}{\pi}\int_0^{\infty} d\omega J(\omega)[\coth(^1/_2\hbar\omega\beta)\cos(\omega t) - i\sin(\omega t)]\end{aligned} \tag{3.5}$$

The coefficients $\eta_{kk'}$ in eq 2.9 are closely related to the trapezoid-rule discretization of the function $\alpha(t-t')$.[28]

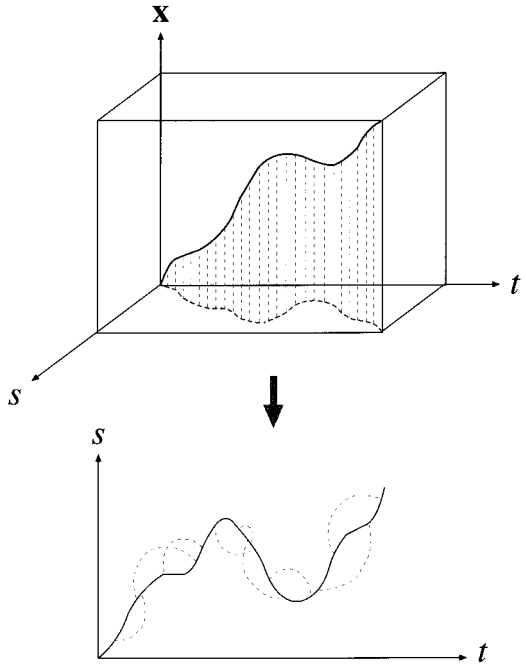

Figure 5. Schematic representation of a Feynman path in full-dimension system−bath space and its projection onto the reduced-dimension space characterized by the system coordinate alone. The gray dashed lines indicate some of the nonlocal influence functional interactions arising from this projection.

It is instructive to point out a formal analogy between the situation at hand and the *classical* dynamics of the system−bath Hamiltonian. Although the classical dynamical variables obey Newton's equations in the phase space of *all* (system and bath) degrees of freedom, elimination of the harmonic bath degrees of freedom again produces[38] a non-Markovian equation of motion for the coordinate of the system of interest known as the generalized Langevin equation (GLE), which for a system described by the Hamiltonian $H_s = p_s^2/2m_0 + V_0(s)$ takes the form

$$m_0\ddot{s}(t) + V_0'(s(t)) + \int_0^t \chi(t-t')\,\dot{s}(t')\,dt' = \zeta(t) \quad (3.6)$$

Here $\chi(t-t')$ is the (generally time-dependent) friction kernel given by the expression

$$\chi(t) = \frac{2}{\pi}\int_{-\infty}^{\infty}\frac{J(\omega)}{\omega}\cos\omega t\,d\omega \quad (3.7)$$

and $\zeta(t)$ is a random force satisfying the second fluctuation-dissipation theorem,[39]

$$\langle\zeta(t)\,\zeta(t')\rangle = k_B T\,\chi(t-t') \quad (3.8)$$

The evolution of the system coordinate is seen from eq 3.6 to depend on the history of the trajectory through the memory kernel $\chi(t-t')$, in close similarity to the quantum path integral situation.

Still, close examination of the influence functional reveals a fundamental difference between classical memory and quantum nonlocality. The nonlocal terms in the path integral expression of the reduced density matrix arise from the correlation function of the medium,[26]

$$\alpha(t-t') = \hbar^{-1}\sum_j c_j^2\langle x_j(t')\,x_j(t)\rangle \quad (3.9)$$

which in the case of a harmonic bath takes the form

$$\alpha(t) = \sum_j \frac{c_j^2}{2m_j\omega_j}[\coth(^1/_2\hbar\omega_j\beta)\cos(\omega_j t) - i\sin(\omega_j t)] \quad (3.10)$$

$$= \frac{1}{\pi}\int_0^\infty J(\omega)[\coth(^1/_2\hbar\omega\beta)\cos(\omega t) - i\sin(\omega t)]\,d\omega$$

The coefficients $\eta_{kk'}$ in eq 2.9 are closely related to the trapezoid-rule discretization of the function $\alpha(t-t')$.[28] It can be shown[40] that the memory arising from a classical bath (i.e., by using the $\hbar \to 0$ limit of the response function) can be eliminated, leading to Markovian evolution. By contrast, the purely imaginary part of the quantum response function prohibits such simplification.

The classical memory kernel arising from dissipative phonon baths usually decays rapidly. This is the result of phase cancellation among a practically infinite number of different frequency modes. As a consequence, the evolution of the system coordinate according to the GLE equation of motion, although not Markovian, is nevertheless governed largely by the frictional forces in the recent history of the trajectory, while the details of the motion in the distant past are of no importance. Assuming that the friction kernel $\chi(t)$ drops below an acceptable threshold within a time length τ, eq 3.6 can be rewritten as

$$m_0\ddot{s}(t) + V_0'(s(t)) + \int_{t-\tau}^t \chi(t-t')\,\dot{s}(t')\,dt' = \zeta(t) \quad (3.11)$$

which requires storing the trajectory over a (short) interval τ preceding the current time.

In analogy with the classical friction kernel, the correlation function for a dissipative bath also decays with time, implying that the nonlocality of the influence functional has in practice a finite span which is equivalent to Δk_{max} path integral time steps. The last observation allows decomposition of the path integral into a series of lower-dimensional integrals.[27,41−44] This is best seen from the diagrammatic representation of the path integral expression, eq 2.8, shown in Figure 6. Here each vertex represents a time point on the forward or backward time axis, while the loops indicate the factors (pairwise interactions) between these points in the path integral. The nearest neighbor interactions correspond to the reference system propagators as well as the influence functional terms having $k' = k - 1$. All other loops indicate other influence functional terms. In this illustration it is assumed that the bath correlation function decays to zero within $\Delta k_{max} = 3$ time steps, leading to omission of loops connecting points separated by a larger time interval. The reduced density matrix at a later time $t = n\Delta k_{max}\Delta t$ is obtained by summing over the quadrature points corresponding to all previous points connected by the appropriate loops (multiplied by the proper initial condition). This operation can also be performed via the procedure outlined below.

First, each forward or backward path in eq 2.8 is decomposed into shorter segments that span the time intervals $0 \le t \le (\Delta k_{max} - 1)\Delta t$, $\Delta k_{max}\Delta t \le t \le (2\Delta k_{max} - 1)\Delta t$, etc. The time points on which these path segments are defined are designated in Figure 6 as vertexes of different colors. Next, one constructs an array of forward and backward path segment pairs, i.e., sequences of $2\Delta k_{max}$ coordinate values on the DVR grid. The assumption that the length of influence functional interactions does not exceed Δk_{max} time steps implies that each path segment is coupled only to its nearest neighbors (see Figure 6). Therefore, a propagator matrix **T** can be constructed whose matrix element T_{ji} consists of all interactions that couple the *i*th path segment to its *j*th neighbor in the direction of increasing

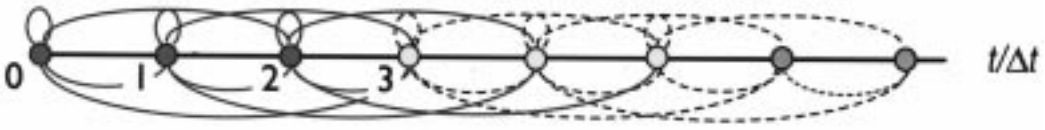

Figure 6. Diagrammatic representation of the path integral interactions (curved lines) in a case where the memory length is equal to three time steps. The circles indicate time points separated by Δt. Red and yellow circles correspond to points defining the matrix **R** of path segments at times 0 and $k\Delta t$ ($k = 3$), respectively. The blue lines indicate the interactions included in the propagator matrix.

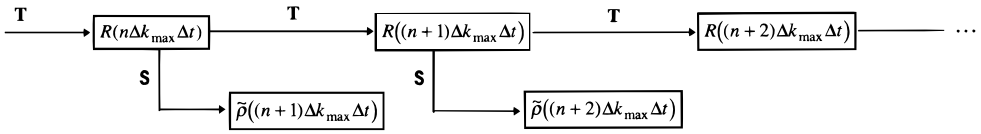

Figure 7. Diagrammatic representation of the procedures involved in the reduced density matrix propagation.

time. To take advantage of this structure, we introduce a *functional* of path segments[43] which corresponds to a multi-time-reduced density matrix. If there are L path segments, this functional becomes a vector **R** of elements

$$R_i(m\Delta k_{\max}\Delta t) \equiv \mathbf{R}((s_1^{\pm},...,s_{\Delta k_{\max}}^{\pm})_i;\, m\Delta k_{\max}\Delta t), \quad i = 1, ..., L \tag{3.12}$$

defined on the time intervals $m\Delta k_{\max}\Delta t \le t < (m+1)\Delta k_{\max}\Delta t$, where m is an integer. This vector can be propagated forward in time via multiplication with the $L\times L$ propagator matrix **T**:

$$\mathbf{R}((m+1)\Delta k_{\max}\Delta t) = \mathbf{T}\cdot\mathbf{R}(m\Delta k_{\max}\Delta t) \tag{3.13}$$

Notice that the matrix **T** is a functional of the earlier and later path segments introduced above. Finally, multiplication by an $M^2\times L$-dimensional endpoint propagator **S** yields[44] the desired reduced density matrix at the discrete times $m\Delta k_{\max}\Delta t$:

$$\tilde{\rho}(m\Delta k_{\max}\Delta t) = \mathbf{S}\cdot\mathbf{R}((m-1)\Delta k_{\max}\Delta t) \tag{3.14}$$

The procedure is summarized in the diagram of Figure 7.

The M DVR states employed in the calculation give rise to a total of $M^{2\Delta k_{\max}}$ forward and backward path segments. Although dramatically smaller than the total number M^{2N} of paths that enter the complete path integral for $N \gg \Delta k_{\max}$, this size of the array **R** is in most cases prohibitive. The crucial observation[45,44] that leads to a tractable scheme exploits the presence of a real part in the exponent of the influence functional. Due to this damping factor, the vast majority of paths enter the path integral with negligible weight and therefore could be neglected. Because of the product structure of the influence functional, a path that spans the long time $N\Delta t$ can have appreciable weight only if *all* of its constituent path segments have weights that are larger than some threshold θ. In general, for $\Delta k_{\max} \gg 1$ the number of path segments with appreciable weight constitutes a very small fraction of the total number $M^{2\Delta k_{\max}}$ of conceivable forward and backward path segments that span the memory length. Therefore, the iterative propagation is preceded by a Monte Carlo random walk in the space of paths with length equal to the memory time which identifies those with weight larger than a preselected threshold; details have been given in ref 44. The L path segments selected from this procedure form the elements of the array **R** introduced above. In many situations typical of electron or proton transfer in the condensed phase the storage requirements of the scheme described above are modest.

During each step in the multiplication process, path segments are pieced together to form longer paths. After n iterations of eq 3.11 the total number of forward/backward paths effectively included is equal to L^{n-1}. For example, a selection of just 10^4 path segments leads after 100 iterations to a result equivalent to that obtainable through explicit summation over 10^{400} system paths. Clearly, inclusion of such an astronomical number of terms through global (noniterative) summation is not a viable alternative.

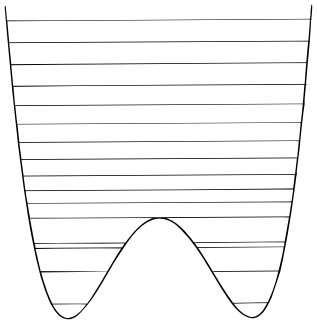

Figure 8. Double-well potential employed in the rate calculations summarized in section IV. The energy spectrum is also shown. (The splitting of the two lowest doublets cannot be discerned.)

IV. Examples

In this section we illustrate the implementation of the path integral methodology presented in this article with two examples. The first involves barrier crossing along a reaction coordinate characterizing a process in a solid material, such as an isomerization reaction or a single site-to-site hop in the diffusion of a hydrogen impurity in a crystalline host. In this case the relevant parameters can be obtained from expansion of the Born−Oppenheimer Hamiltonian in terms of the small-amplitude lattice vibrations about the reaction path. The second case deals with electron transfer in a biological environment. Here the process is dominated by nonadiabatic transitions between the potential surfaces characterizing the charge-transfer states. As the liquid and protein modes undergo large-amplitude motion, quadratic expansions about a reference geometry are not meaningful and the spectral density is inferred from the classical correlation function of the energy gap which is obtained via molecular dynamics simulations.

(a) Tunneling in Isomerization Reactions. The first illustration of the path integral scheme described in sections II and III is its application to a generic model of barrier crossing, such as the transfer of a hydrogen atom between two equivalent sites in a condensed-phase medium. The system Hamiltonian is chosen as a symmetric double-well potential with a barrier of 6 kcal/mol. This potential, along with a few of the lowest eigenenergies, is shown in Figure 8. The process of interest is

the transfer between the two potential minima through a combination of activated dynamics and tunneling.

Under the most common conditions, the reactant population in the process described above exhibits exponential decay whose rate is determined by the interplay among several relevant time scales: first, one has the "gas-phase" time constants, i.e., the period of vibration in the potential wells and the time associated with tunneling in the lowest doublet. Also of importance are the relaxation time of the medium as well as the overall time constant of the reaction. At the temperatures of interest the time required for completion of the reaction is much larger than all vibrational periods due to the low Boltzmann-weighted probability of overcoming the barrier, and the process is governed by the statistics of rare events (see, for example, ref 46).

Rather than following the dynamics of the reactant population over the very long time required to observe formation of products, a more efficient calculation of the reaction rate is via the reactive flux method.[47−51] This method obtains the rate by calculating the time-integrated reactive flux through a fictitious dividing surface separating reactants from products. In the quantum reactive flux formalism of Miller et al. the rate is proportional to the time integral of the flux−flux correlation function[52]

$$C_f(t) = \mathrm{Tr}(\bar{F}e^{iHt_c^*/\hbar}\bar{F}e^{-iHt_c/\hbar}) \tag{4.1}$$

Here

$$\bar{F} = \frac{1}{2m}(p_s\delta(s - s_0) + \delta(s - s_0)p_s) \tag{4.2}$$

is the symmetrized flux operator which measures the reactive flux through a dividing surface located at $s = s_0$, $t_c = t - i\hbar\beta/2$ is a complex time that arises from combining the time-evolution operator with the symmetrically split Boltzmann operator, and the correlation function is integrated up to the "plateau" time, which is long compared to vibrational periods in the stable well but generally much shorter than the time required for completion of the reaction. As a consequence, calculation of the reaction rate according to the reactive flux formalism requires only short time dynamics.

If the interaction forces between the quantum particle and the crystal atoms are available, the phonon frequencies and coupling functions can be obtained from a quadratic expansion of the potential about the reaction path. While simulation of a specific reaction requires a numerical calculation of the individual coupling functions, a simple generic model can capture the important qualitative aspects of the dynamics. A useful model emerges from the Debye spectrum, which predicts a density of states that grows as ω^{d-1} at small frequencies, where d is the dimension of the solid, while terminating at some characteristic Debye frequency. Use of the deformation potential approximation (see, for example, ref 53) results in a spectral density of the type ω^d. Introducing a smooth exponential cutoff for the high-frequency part of the spectrum leads to the following popular model for the spectral density:[54]

$$J(\omega) = \gamma\omega\left(\frac{\omega}{\omega_c}\right)^{d-1}e^{-\omega/\omega_c} \tag{4.3}$$

Here γ is a friction parameter characterizing the overall strength of coupling to the phonons. Below we focus on the so-called Ohmic case obtained from eq 4.3 with $d = 1$, which displays the most diverse behaviors.

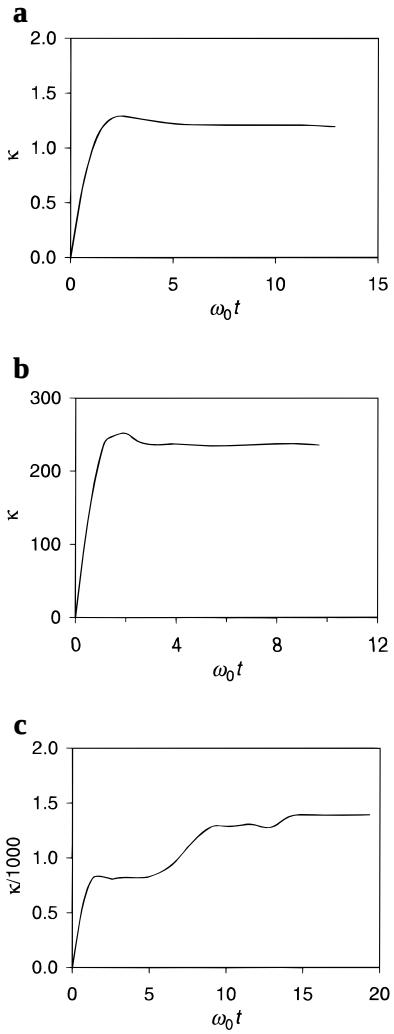

Figure 9. Path integral results for the time integral of the flux−flux correlation function for the reaction described by the double-well potential discussed in the text: (a) $\beta E_b = 10$ (activated regime), strong friction; (b) $\beta E_b = 10$ (activated regime), weak friction; (c) $\beta E_b = 30$ (deep tunneling regime, weak friction).

Obtaining the quasi-adiabatic propagator path integral representation of the flux correlation function is straightforward and leads to a $2N-2$-dimensional integral.[29] Since knowledge of the flux correlation function for relatively short times determines the reaction rate, it is possible to obtain the latter via a combination of Monte Carlo sampling and multidimensional DVR quadrature, without resorting to the iterative procedure described in section III.

In the temperature range considered in Figure 10 below ($\beta E_b \sim 10-30$) convergence of the flux correlation function is achieved with $N \leq 8$. At the lowest of these temperatures and with sufficiently strong system−bath coupling the damping is significant and the Monte Carlo procedure outlined in section II converges fairly rapidly. By contrast, at higher temperatures and/or weak coupling the oscillations in the integrand are more severe, necessitating the use of multidimensional DVR quadrature with $M \leq 16$. Typical behaviors of the integrated flux correlation function are shown in Figure 9. The upward or downward step structure is associated with constructive or destructive phase interference arising from recurrences of the quantum flux on the time scale of vibration in the reactant well.[55] These recurrences, whose origin is strictly quantum mechani-

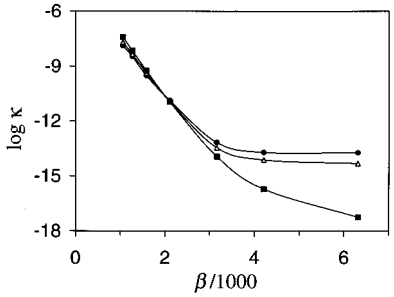

Figure 10. Logarithm of the rate constant for the model reaction discussed in the text as a function of inverse temperature. Blue line: very weak friction, $\gamma/\omega_b = 0.05$. Green line: weak friction, $\gamma/\omega_b = 0.1$. Red line: moderate friction, $\gamma/\omega_b = 0.5$.

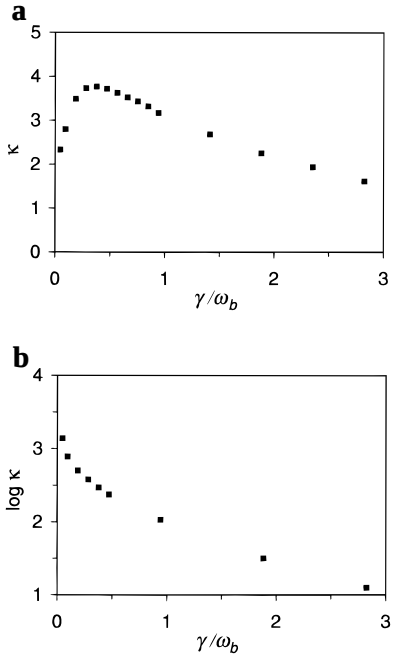

Figure 11. Path integral results for the quantum transmission coefficient of the model double-well potential discussed in the text as a function of system−bath coupling strength. (a) Temperature above crossover, $\beta E_b = 15$. (b) Temperature around crossover, $\beta E_b = 30$. Values of γ/ω_b greater than approximately 0.6 correspond to activated dynamics, while tunneling effects become dominant at smaller values of the friction.

cal,[56] lead to large deviations of the quantum rate compared to that predicted by imaginary-time transition-state-like models.[57]

Figure 10 shows an Arrhenius plot of the calculated rate constant over a wide range of temperatures at three values of the friction strength. All three curves show the expected crossover from the activated regime to that dominated by quantum tunneling. This transition is seen to be sharper for weak coupling to the phonon bath, while nonnegligible dependence on temperature in the deep tunneling regime is observed with stronger coupling, in agreement with semiclassical predictions.[58] In addition, the crossover temperature shifts to lower values as the coupling strength is increased.

Finally, the dependence of the rate on system−bath coupling strength is shown in Figure 11 for two temperatures. Plotted here is the quantum transmission coefficient, i.e., the rate constant divided by the estimate of classical transition-state theory. The rate constant displays the well-known Kramers turnover[59] in the activated regime, and the simulation results are in excellent agreement with earlier theoretical work.[60,61] As the temperature is lowered, the characteristic friction at turnover

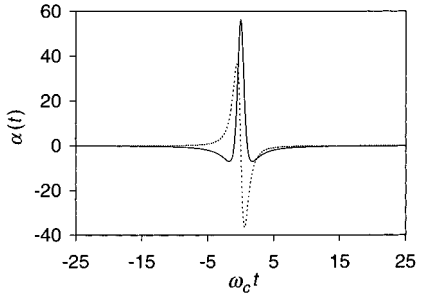

Figure 12. Real (solid line) and imaginary parts (dashed line) of the bath response function for the spectral density given by eq 4.3 with $d = 1$.

shifts to smaller values. In the deep tunneling regime approximate treatments are only qualitatively correct. At sufficiently low temperature the rate dependence on friction is for all practical purposes monotonic.

At very low temperatures the dynamics is dominated by the characteristics of the tunneling doublet, and the problem reduces to the spin-boson model (dissipative two-level system), which has been the subject of numerous studies. In this case the system Hamiltonian can be expressed in the form

$$H_s = -\hbar\Omega\begin{pmatrix} 0 & 1 \\ 1 & 0 \end{pmatrix} \tag{4.4}$$

where Ω is equal to half of the tunneling frequency. Depending on the values of the temperature and the friction strength, the spin-boson Hamiltonian exhibits a variety of behaviors, which include underdamped or incoherent relaxation and even complete localization.[54] These behaviors are commonly summarized in terms of the dimensionless Kondo parameter $\xi = 2\gamma/\pi\hbar$.

In order to examine the diverse dynamics of the dissipative two-level system, the reduced density matrix must be integrated over sufficiently long time intervals. Numerical results obtained with the iterative path integral procedure of section III are presented below for an Ohmic bath characterized by $\omega_c = 10\Omega$ for $\hbar\Omega/k_BT$ ranging between 0.1 and 5 and with weak to moderate friction strength. In this range of parameters the path integral converges with time steps $\Delta t \sim 0.03-0.08\ \Omega^{-1}$. In order to obtain an estimate of the characteristic memory time, one must examine the bath response function. Figure 12 shows this function for the case of the spectral density characterized by eq 4.3. It is seen that the real and imaginary parts of the response function decay to values close to zero within 4−8 time steps. With this memory length the number $L = 2^{2\Delta k_{max}}$ of path segments is modest and no path selection is necessary. (However, further decomposition of the propagator matrix is now required.[41])

Typical behaviors of the average two-level system position are shown in Figure 13. In accord with the predictions of the noninteracting blip approximation,[54] this quantity displays exponential decay at high temperature and/or sufficiently strong friction parameter. At low temperatures and small values of the Kondo parameter the system undergoes underdamped oscillations and eventually achieves its equilibrium value.

(b) Biological Charge Transfer. Electron transfer is intrinsically a classically forbidden phenomenon, requiring structural transformations that are not compatible with the potential governing a single Born−Oppenheimer state. To model an electron-transfer process, one must be able to describe the quantum dynamics of the nuclear motion associated with curve-crossing events as well as quantum tunneling. Here we employ the common picture where the nuclear dynamics of the donor

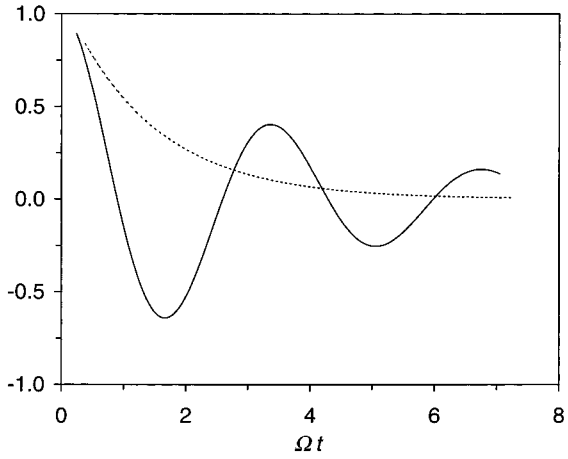

Figure 13. Average position of a two-level system coupled to a bath with the spectral density described in the text as a function of time for various combinations of temperature and friction strength. Dashed line: $\hbar\Omega\beta = 0.1$, $\xi = 0.2$. Solid line: $\hbar\Omega\beta = 5$, $\xi = 0.1$.

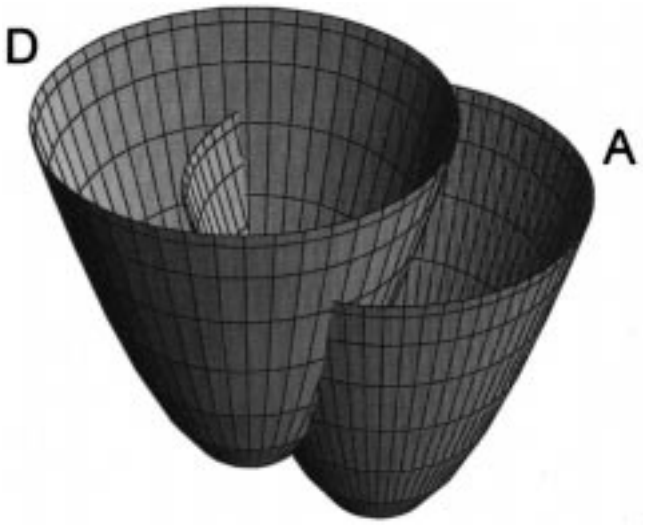

Figure 14. Sketch of the multidimensional free energy surfaces of the donor and acceptor in an electron-transfer process.

and acceptor states is described by two multidimensional diabatic potential wells. If the medium is characterized by large-amplitude floppy motion, as in the case of electron transfer in solution or in a biological host, the donor and acceptor potential surfaces are expected to be very anharmonic functions of the atomic displacements. However, the process of electron transfer is governed by the *collective* motion of a large number of solvent coordinates. As such, use of the central limit theorem implies a Gaussian response, such that the dynamics induced by the actual multidimensional anharmonic medium is equivalent to that of an effective harmonic bath of an appropriate spectral density.[2,56,62−65] With this simplification the process is modeled by eq 1.1 where H_s is now a Hamiltonian matrix whose diagonal elements are the free energies of the relevant charge-transfer states. A sketch of the parabolic free energy surfaces is given in Figure 14.

The collective characteristics of the solvent or biological medium can be mapped onto those specifying the system−bath model by invoking the quantum classical correspondence for harmonic oscillators. Specifically, as the nuclear degrees of freedom (modeled as classical variables) fluctuate about their equilibrium configuration, the energy gap between the donor and acceptor states fluctuates about its average value as the function

$$\text{const} + l\sum_j c_j x_j^{\text{cl}}(t) \tag{4.5}$$

where $x_j^{\text{cl}}(t)$ denote the classical coordinates and l is a constant determined by the donor−acceptor distance in the Hamiltonian. The correlation function $C_{\text{DA}}(t)$ of the donor−acceptor energy gap fluctuations about its equilibrium average is then

$$C_{\text{DA}}(t) = l^2\sum_j c_j^2\langle x_j^{\text{cl}}(0)\, x_j^{\text{cl}}(t)\rangle_\beta \tag{4.6}$$

Noting that $C_{\text{DA}}(t)$ is simply related to the classical limit of the response function,

$$C_{\text{DA}}(t) = l^2 \lim_{\hbar\to 0}\hbar\alpha(t) \tag{4.7}$$

the gap fluctuation correlation function can be expressed in terms of the spectral density according to the relation

$$C_{\text{DA}}(t) = \frac{2l^2}{\pi\beta}\int_0^\infty \frac{J(\omega)}{\omega}\cos\omega t\, \mathrm{d}\omega \tag{4.8}$$

which can be inverted to yield the spectral density as the Fourier integral

$$J(\omega) = \frac{\beta\omega}{l^2}\int_0^\infty C_{\text{DA}}(t)\cos\omega t\, \mathrm{d}t \tag{4.9}$$

Thus, the collective characteristics of the medium relevant to the electron-transfer process can be found from the Fourier transform of the classical gap fluctuation correlation function, which is obtainable via classical molecular dynamics simulations.

As an illustrative example, we discuss below the path integral simulation of the primary charge separation in bacterial photosynthetic reaction centers. The process starts with photoexcitation of a special chlorophyll pair, denoted P, which initiates a series of electron-transfer reactions whose earliest detectable product is a negatively charged bacteriopheophytin H_L located about 17 Å away on the L side of the polypeptide.[66] (See Figure 15.) This process has a time constant of 3 ps and is believed to be mediated by an accessory bacteriochlorophyll B_L located between the primary donor and acceptor units. In agreement with some earlier theoretical predictions,[67−69] there is now strong evidence[70−73] that the reduced accessory chlorophyll state participates in the electron transfer as part of a two-step process characterized by a fast second kinetic step which does not allow detectable accumulation of electron charge on this monomer.[74−80] The corresponding arrangement of the diabatic free energy surfaces is sketched in Figure 16.

The process has been modeled via a three-state Hamiltonian which is coupled to a dissipative medium of protein and water modes via a spectral density that is obtained from classical molecular dynamics simulations.[81] The spectral density function is reproduced in Figure 17 along with the corresponding bath response function. The path integral time step varies between 3 and 13 fs, such that the medium-induced memory spans up to 35 time steps. The total simulation time ranges between 2000 and 5000 time steps. A Monte Carlo path selection is carried out, reducing the number of statistically significant path segments from the total number $L = 3^{70}$ to about 10^4-10^5.

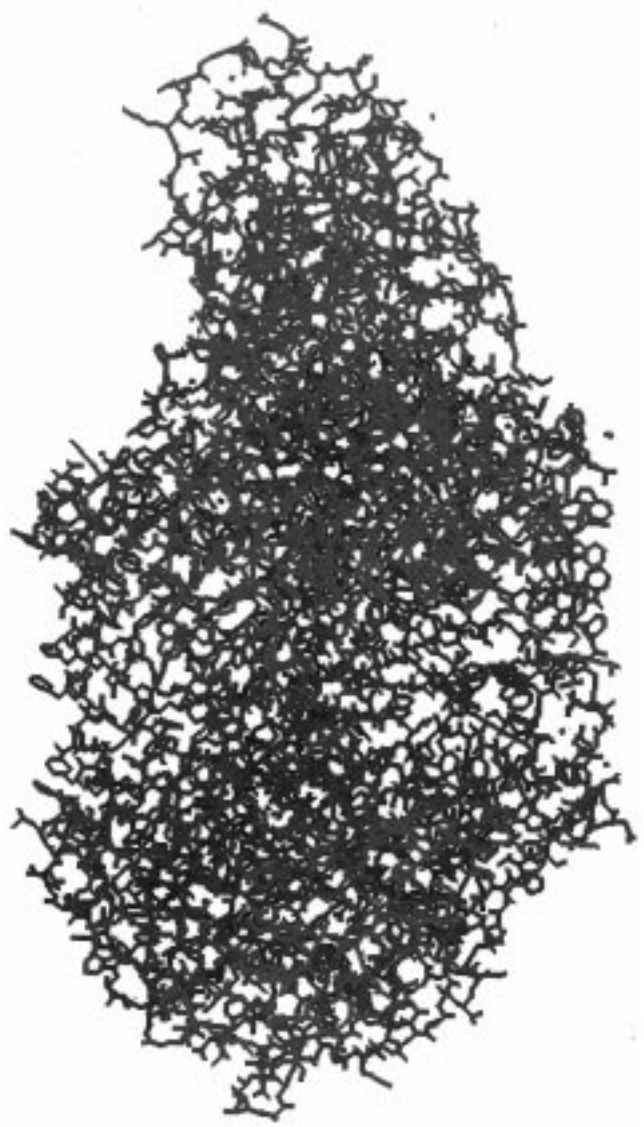

Figure 15. Three-dimensional view of the bacterial photosynthetic reaction center of *Rps. viridis*. The bacteriochlorophyll and bacteriopheophytin groups are shown in red.

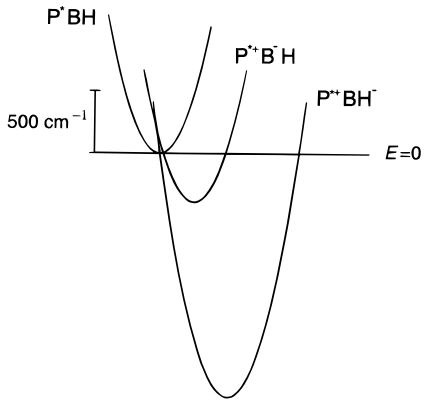

Figure 16. Schematic representation of the diabatic surfaces corresponding to the bacteriochlorophyll special pair, the reduced bacteriochlorophyll monomer, and the reduced bacteriopheophytin in the photosynthetic reaction center of *Rps. viridis.*

The evolution of the electronic state populations is shown in Figure 18. The simulation results can be fitted well by a two-step kinetic equation:

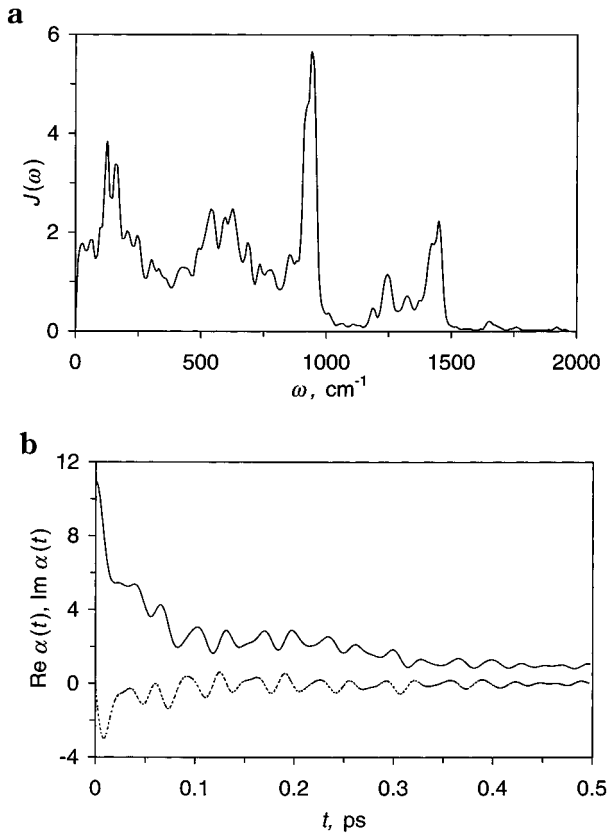

Figure 17. Protein and solvent features affecting the dynamics of primary charge separation in the photosynthetic reaction center of *Rps. viridis.* (a) Spectral density obtained via molecular dynamics simulations in ref 81. (b) Bath response function $\alpha(t)$ at 300 K. The solid and dotted lines correspond to the real and imaginary parts of this function.

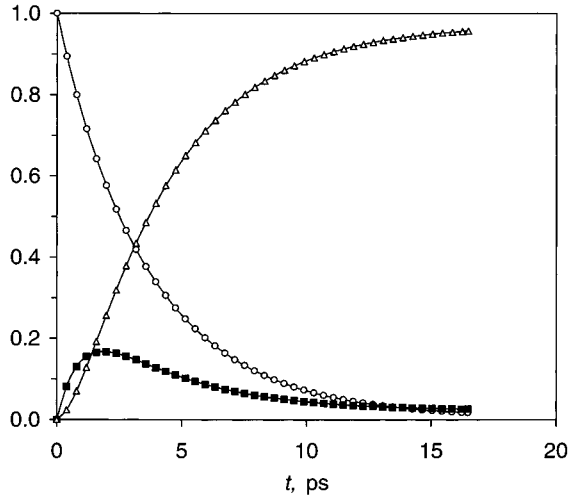

Figure 18. Evolution of the electronic state populations for the wild-type reaction center obtained via iterative propagation of the reduced density matrix. The free energy of the reduced accessory bacteriochlorophyll is 400 cm^{-1} lower than that of the donor. The donor−bridge and bridge−acceptor couplings are set equal to 22 and 135 cm^{-1}, respectively. Hollow circles: population of the electron donor. Filled squares: population of the bridge. Hollow triangles: population of the electron acceptor. (Data from ref 73.)

$$P^*B_LH_L \underset{k_{-1}}{\overset{k_1}{\rightleftharpoons}} P^{*+}B_L^-H_L \underset{k_{-2}}{\overset{k_2}{\rightleftharpoons}} P^{*+}B_LH_L^- \qquad (4.10)$$

Additional path integral simulations have confirmed that the two-step model with the determined parameters[72] reproduces

well the temperature dependence observed on the wild-type reaction center as well as the modified kinetics of certain studied mutants.

V. Summary and Outlook

The path integral methodology described in this article offers the attractive possibility of allowing fully quantum mechanical simulations of dynamical processes in dissipative phonon-type environments. No ad hoc assumptions about the evolution are introduced, leading to reliable results in parameter regimes not accessible by available analytic or numerical approximations.

Depending on the situation at hand, the parameters in the Hamiltonian of eq 1.1 can be specified either in terms of the individual phonon frequencies and coupling functions obtainable through a Taylor expansion of the multidimensional potential energy surface or from the collective characteristics of the bath encoded in its correlation function; in turn, the latter can be calculated by means of classical molecular dynamics methods, thus providing the information necessary for mapping anharmonic media onto effective harmonic models under conditions leading to Gaussian response.

Unlike earlier approaches to real-time path integration which were based on Monte Carlo evaluation of the highly oscillatory path integral expression discretized in terms of primitive propagators, the present scheme takes advantage of the physics of the process in multiple ways to achieve a viable algorithm: First, a physically motivated reference is employed in the discretization of the short time propagator, leading to a path integral representation which incorporates the exact dynamics along the adiabatic path as its zeroth-order limit. Second, the finite-basis eigenstate expansion of the reference propagator filters out the rapid phase oscillations of the latter, resulting in a well-behaved integrand. Third, the use of system-specific discrete variable representations of the path integral in the bulk of parameter space provides the most economical quadrature, leading to a dramatic contraction of the required multidimensional grid. Lastly, exploiting the finite extent of nonlocal interactions in the resulting influence functional associated with dissipative baths encountered in the condensed phase allows decomposition of the path integral into a series of low-dimensional operations, leading to an iterative algorithm that does not suffer from the alternating sign problem.

The DVR-discretized quasi-adiabatic propagator path integral and the iterative procedure discussed in sections II and III lead to numerically exact results once convergence with respect to step size, number of quadrature terms, memory length, and path segment acceptance threshold has been reached. The examples presented in section IV provide a feel for the magnitude of these parameters.

The availability of a numerically exact scheme for simulating the dynamics of systems described by a reaction coordinate interacting with a collection of harmonic bath degrees of freedom opens up the way to exploring a host of chemically interesting questions such as hydrogen atom or electron transfers in solution or in biological environments, structural isomerizations, or light particle diffusion on solid surfaces or in the bulk, to name but a few. Further, the methodology reviewed in this article is easily generalizable to Hamiltonians including time-dependent fields, allowing its application to systems interacting with coherent laser radiation. Some of these questions have been explored in recent articles.[82−86]

Yet, quantum molecular dynamics, the ability to follow the dynamics of large molecules with the same rigor that characterizes routine classical trajectory simulations, remains out of reach. This goal has been a long-standing dream of many theoretical chemists, as there are numerous chemically interesting situations that are too complex to allow decomposition of the Hamiltonian into a system coupled to a harmonic bath. At the moment it appears that the most general many-body quantum dynamics problem is not amenable to numerically exact solution due to the exponential scaling of the quantum mechanical equations of motion with system size. Nevertheless, it is likely that ideas similar in spirit to those employed in this article can lead to numerically tractable, yet sufficiently rigorous techniques for treating processes in nearly classical anharmonic fluids or other similar situations. Such goals will undoubtedly attract significant attention in the future.

Acknowledgment. The work reviewed in this article has been possible through the generous support of several agencies. I wish to thank the Arnold and Mabel Beckman Foundation for a Beckman Young Investigator Award, the David and Lucile Packard Foundation for a Packard Fellowship for Science and Engineering, the National Science Foundation for a Young Investigator Award, for Grant No. 93-13603, and for funding through the University of Illinois Materials Research Laboratory, the Alfred Sloan Foundation for a Sloan Research Fellowship, the Research Corporation for a Cottrell Scholar Award, and the Camille and Henry Dreyfus Foundation for a Camille Dreyfus Award.

References and Notes

(1) Feynman, R. P. *Rev. Mod. Phys.* **1948**, *20*, 367−387.
(2) Feynman, R. P.; Hibbs, A. R. *Quantum Mechanics and Path Integrals*; McGraw-Hill: New York, 1965.
(3) Thirumalai, D.; Berne, B. J. *J. Chem. Phys.* **1983**, *79*, 5029−5033.
(4) Galliccio, E.; Berne, B. J. *J. Chem. Phys.* **1994**, *101*, 9909−9918.
(5) Galliccio, E.; Berne, B. J. *J. Chem. Phys.* **1996**, *105*, 7064−7078.
(6) Behrman, E. C.; Jongeward, G. A.; Wolynes, P. G. *J. Chem. Phys.* **1983**, *79*, 6277−6281.
(7) Behrman, E. C.; Wolynes, P. G. *J. Chem. Phys.* **1985**, *83*, 5863−5869.
(8) Cline, R. E., Jr.; Wolynes, P. G. *J. Chem. Phys.* **1988**, *88*, 4334−4350.
(9) Mason, B. A.; Hess, K.; Cline, R. E.; Wolynes, P. G. *Superlattices Microstruct.* **1987**, *3*, 421−428.
(10) Krempl, S.; Winterstetter, M.; Domcke, W. *J. Chem. Phys.* **1995**, *102*, 6499−6510.
(11) Mak, C. H. *Phys. Rev. Lett.* **1992**, *68*, 899−902.
(12) Mak, C. H.; Egger, R. *Adv. Chem. Phys.* **1996**, *XCIII*, 39−76.
(13) Filinov, V. S. *Nucl. Phys. B* **1986**, *271*, 717−725.
(14) Makri, N.; Miller, W. H. *Chem. Phys. Lett.* **1987**, *139*, 10−14.
(15) Makri, N.; Miller, W. H. *J. Chem. Phys.* **1988**, *89*, 2170−2177.
(16) Doll, J. D.; Freeman, D. L. *Adv. Chem. Phys.* **1988**, *73*, 289−304.
(17) Doll, J. D.; Freeman, D. L.; Gillan, M. J. *Chem. Phys. Lett.* **1988**, *143*, 277.
(18) Doll, J. D.; Freeman, D. L.; Beck, T. L. *Adv. Chem. Phys.* **1990**, *78*, 61.
(19) Mak, C.; Chandler, D. *Phys. Rev. A* **1990**, *41*, 5709−5712.
(20) Mak, C. H.; Chandler, D. *Phys. Rev. A* **1991**, *44*, 2352−2369.
(21) Makri, N. *Chem. Phys. Lett.* **1989**, *159*, 489−498.
(22) Makri, N. *J. Chem. Phys.* **1992**, *97*, 2417−2424.
(23) Sharafeddin, O. A.; Kouri, D. J.; Nayar, N.; Hoffman, D. *J. Chem. Phys.* **1991**, *95*, 3224−3231.
(24) Winterstetter, M.; Domcke, W. *Chem. Phys. Lett.* **1995**, *236*, 445−450.
(25) Makri, N. *Chem. Phys. Lett.* **1992**, *193*, 435−444.
(26) Feynman, R. P.; F. L. Vernon, J. *Ann. Phys.* **1963**, *24*, 118−173.
(27) Makri, N.; Makarov, D. E. *J. Chem. Phys.* **1995**, *102*, 4600−4610.
(28) Makri, N. *J. Math. Phys.* **1995**, *36*, 2430−2456.
(29) Topaler, M.; Makri, N. *Chem. Phys. Lett.* **1993**, *210*, 285−293.
(30) Harris, D. O.; Engerholm, G. G.; Gwinn, W. D. *J. Chem. Phys.* **1965**, *43*, 1515−1517.
(31) Dickinson, A. S.; Certain, P. R. *J. Chem. Phys.* **1968**, *49*, 4209−4211.
(32) Light, J. C.; Hamilton, I. P.; Lill, J. V. *J. Chem. Phys.* **1985**, *82*, 1400−1409.

(33) Lill, J. V.; Parker, G. A.; Light, J. C. *Chem. Phys. Lett.* **1982**, *89*, 483−489.
(34) Bačić, Z.; Light, J. C. *Annu. Rev. Phys. Chem.* **1989**, *40*, 469−498.
(35) Colbert, D. T.; Miller, W. H. *J. Chem. Phys.* **1992**, *96*, 1982−1991.
(36) Topaler, M.; Makri, N. *Chem. Phys. Lett.* **1993**, *210*, 448.
(37) Sim, E.; Makri, N. *J. Chem. Phys.* **1995**, *102*, 5616−5625.
(38) Zwanzig, R. *J. Stat. Phys.* **1973**, *9*, 215−220.
(39) Kubo, R.; Toda, M.; Hashitsume, N. *Statistical Physics*, 2nd ed.; Springer-Verlag: Heidelberg, 1991; Vol. 2.
(40) Makri, N. *J. Chem. Phys.* (in press).
(41) Makri, N.; Makarov, D. E. *J. Chem. Phys.* **1995**, *102*, 4611−4618.
(42) Makarov, D. E.; Makri, N. *Chem. Phys. Lett.* **1994**, *221*, 482−491.
(43) Makri, N. Path integral simulation of long-time dynamics in quantum dissipative systems. In *Path Integrals: Basics and Applications*; DeWitt-Morette, C., Ed.; Plenum: New York, 1997.
(44) Sim, E.; Makri, N. *Comput. Phys. Commun.* **1997**, *99*, 335−354.
(45) Sim, E.; Makri, N. *Chem. Phys. Lett.* **1996**, *249*, 224−230.
(46) *Activated Barrier Crossing*; Fleming, G. R., Hänggi, P., Eds.; World Scientific: Singapore, 1993.
(47) Keck, J. C. *J. Chem. Phys.* **1960**, *32*, 1035.
(48) Kapral, R. *J. Chem. Phys.* **1972**, *56*, 1842.
(49) Chandler, D. *J. Chem. Phys.* **1978**, *68*, 2959−2970.
(50) Berne, B. J. In *Multiple Time Scales*; Brackbill, J. U., Cohen, B. I., Eds.; Academic Press: New York, 1985; p 419.
(51) Yamamoto, T. *J. Chem. Phys.* **1960**, *33*, 281−289.
(52) Miller, W. H.; Schwartz, S. D.; Tromp, J. W. *J. Chem. Phys.* **1983**, *79*, 4889−4898.
(53) Kittel, C. *Quantum theory of Solids*, 2nd ed.; John Wiley & Sons: New York, 1987.
(54) Leggett, A. J.; Chakravarty, S.; Dorsey, A. T.; Fisher, M. P. A.; Garg, A.; Zwerger, M. *Rev. Mod. Phys.* **1987**, *59*, 1−85.
(55) Topaler, M.; Makri, N. *J. Chem. Phys.* **1994**, *101*, 7500−7519.
(56) Onuchic, J. N.; Wolynes, P. G. *J. Phys. Chem.* **1988**, *92*, 6495−6503.
(57) Voth, G. A. *Adv. Chem. Phys.* **1996**, *XCIII*, 135.
(58) Grabert, H.; Weiss, U.; Hanggi, P. *Phys. Rev. Lett.* **1984**, *52*, 2193.
(59) Kramers, H. A. *Physica (Utrecht)* **1940**, *7*, 284−304.
(60) Hänggi, P.; Pollak, E.; Grabert, H. The quantum Kramers problem. The University of Augsburg, 1989.
(61) Rips, I.; Pollak, E. *Phys. Rev. A* **1990**, *41*, 5366−5382.
(62) Marcus, R. A. *J. Chem. Phys.* **1956**, *24*, 966−978.
(63) Marcus, R. A.; Sutin, N. *Biochim. Biophys. Acta* **1985**, *811*, 265−322.
(64) Onuchic, J. N.; Wolynes, P. G. *J. Chem. Phys.* **1993**, *98*, 2218−2224.
(65) Marcus, R. A. *Angew. Chem., Int. Ed. Engl.* **1993**, *32*, 1111−1121.
(66) Deisenhofer, J.; Epp, O.; Miki, K.; Huber, R.; Michel, H. *Nature (London)* **1985**, *318*, 618−624.
(67) Marcus, R. A. *Chem. Phys. Lett.* **1987**, *133*, 471−477.
(68) Marcus, R. A. *Chem. Phys. Lett.* **1988**, *146*, 13−21.
(69) Creighton, S.; Hwang, J. K.; Warshel, E.; Parson, W. W.; Norris, J. *Biochemistry* **1988**, *27*, 774−781.
(70) Schmidt, S.; Arlt, T.; Hamm, P.; Huber, H.; Nagele, T.; Wachtveitl, J.; Meyer, M.; Scheer, H.; Zinth, W. *Chem. Phys. Lett.* **1994**, *223*, 116−120.
(71) Huber, H.; Meyer, M.; Nagele, T.; Hartl, I.; Scheer, H.; Zinth, W.; Wachtveitl, J. *Chem. Phys.* **1995**, *197*, 297−305.
(72) Makri, N.; Sim, E.; Makarov, D. E.; Topaler, M. *Proc. Natl. Acad. Sci. U.S.A.* **1996**, *93*, 3926−3931.
(73) Sim, E.; Makri, N. *J. Phys. Chem.* **1997**, *101*, 5446−5458.
(74) Holten, D.; Hoganson, C.; Windsor, M. W.; Schenck, C. C.; Parson, W. W.; Migus, A.; Fork, R. L.; Shank, C. V. *Biochim. Biophys. Acta* **1980**, *592*, 461−477.
(75) Woodbury, N. W.; Becker, M.; Middendorf, D.; Parson, W. W. *Biochemistry* **1985**, *24*, 7516−7521.
(76) Martin, J.-L.; Breton, J.; Hoff, A. J.; Migus, A.; Antonetti, A. *Proc. Natl. Acad. Sci. U.S.A.* **1986**, *83*, 957−961.
(77) Breton, J.; Martin, J. L.; Petrich, J.; Migus, A.; Antonetti, A. *FEBS Lett.* **1986**, *209*, 37−43.
(78) Breton, J.; Martin, J.-L.; Fleming, G. R.; Lambry, J.-C. *Biochemistry* **1988**, *27*, 9276−8284.
(79) Fleming, G. R.; Martin, J. L.; Breton, J. *Nature (London)* **1988**, *333*, 190−192.
(80) Chan, C.-K.; DiMagno, T. J.; Chen, L. X.-Q.; Norris, J. R.; Fleming, G. R. *Proc. Natl. Acad. Sci. U.S.A.* **1991**, *88*, 11202−11206.
(81) Marchi, M.; Gehlen, J. N.; Chandler, D.; Newton, M. *J. Am. Chem. Soc.* **1993**, *115*, 4178−4190.
(82) Forsythe, K.; Makri, N. *J. Chem. Phys.* **1998**, *108*, 6819−6828.
(83) Makarov, D. E.; Makri, N. *Phys. Rev. B* **1995**, *52*, R2257−2260.
(84) Makri, N.; Wei, L. *Phys. Rev. E* **1997**, *55*, 2475−2478.
(85) Makri, N. *J. Chem. Phys.* **1997**, *106*, 2286−2297.
(86) Taft, G.; Makri, N. *J. Phys. B* **1998**, *31*, 209−226